Available online at www.sciencedirect.com

ScienceDirect

Mendeleev Commun., 2022, **32**, 672–674

Mendeleev Communications

Catalytic synthesis of isoprenol from fatty acid ester over bimetallic Cu–Fe catalysts

Anastasiya A. Shesterkina,*[a,b,c] Anna A. Strekalova,[a,b] Elena V. Shuvalova,[a] Gennady I. Kapustin,[a] Olga P. Tkachenko[a] and Leonid M. Kustov[a,b,c]

[a] *N. D. Zelinsky Institute of Organic Chemistry, Russian Academy of Sciences, 119991 Moscow, Russian Federation. E-mail: anastasiia.strelkova@mail.ru*
[b] *National University of Science and Technology 'MISIS', 119049 Moscow, Russian Federation*
[c] *Department of Chemistry, M. V. Lomonosov Moscow State University, 119991 Moscow, Russian Federation*

DOI: 10.1016/j.mencom.2022.09.035

Supported bimetallic Cu–Fe catalysts revealed high activity and selectivity in isoprenyl acetate hydrogenation to isoprenol under mild reaction conditions (2 MPa H_2 and 170 °C). The nature of the carrier has a significant impact on the catalytic properties of Cu–Fe catalysts. The best catalytic properties were found for the 5% Cu–5% Fe/Al_2O_3 bimetallic catalyst, which provides a 98% isoprenyl acetate conversion in 4 h with the isoprenol selectivity of 82%.

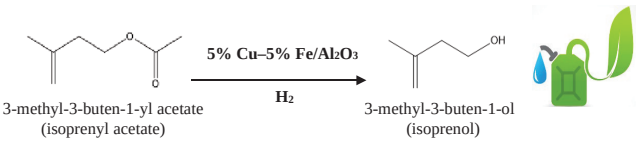

Keywords: hydrogenation, bimetallic catalyst, isoprenol, isoprenyl acetate, iron catalyst, copper catalyst, nanoparticles.

Biofuels obtained from isoprenoids and fatty acids are potential candidates for replacing diesel and jet fuels due to their favorable physicochemical (such as freezing point) and combustion properties (such as cetane number and energy density).[1–5] Recently, isoprenol (3-methyl-3-butene-1-ol), the isoprenoid compound, has attracted particular interest because it is a valuable drop-in biofuel and an important precursor for various biosynthetic pathways and lubricants.[6,7] In addition, isoprenoids, their derivatives and isoprenoid-based food supplements have an ever-increasing impact on human health as they have shown positive effects on combat aging and age-related ailments.[7] It is known that copper-containing catalysts are effective traditional catalytic systems for hydrogenation of esters to respective alcohols, though they are active only at the high temperatures (200–250 °C) and H_2 pressure of 3–5 MPa.[8–10] However, the hydrogenation of unsaturated fatty acid esters to unsaturated alcohols is complicated by the presence of a C=C bond, since the hydrogenation of C=C bonds is more thermodynamically advantageous than the hydrogenolysis of the C–O bond. To date, the use of heterogeneous catalysts for the hydrogenation of unsaturated esters is limited due to the use of high pressures and temperatures, which results in low selectivity of the formation of unsaturated alcohols.

Thus, the aims of our work were to develop effective and selective supported copper-containing catalysts, to study the effect of additives of the second non-noble metal (Fe) on hydrogenation of unsaturated fatty acid esters, in particular isoprenyl acetate, to unsaturated alcohols, *i.e.* isoprenol, and to investigate the effect of the SiO_2 and Al_2O_3 carriers on the catalytic properties of prepared catalysts.

In this work, the synthesis of the supported bicomponent Cu–Fe catalysts has been carried out.† The prepared catalysts were explored in liquid-phase isoprenyl acetate hydrogenation using methanol as a solvent under optimal conditions: 2 MPa H_2 pressure and 170 °C. The products of isoprenyl acetate hydrogenation on mono- and bimetallic Cu–Fe samples were isoprenol and the product of the esterification process, methyl acetate; the carbon balance reached 100%. The results of the catalytic experiments performed on supported Cu–Fe catalysts showed that the addition of iron to copper resulted in the change of their activity and selectivity. The conversion of the substrate on bimetallic Cu–Fe catalysts was achieved in 4 h in comparison

† Bicomponent supported 5% Cu–5% Fe catalysts were synthesized by simultaneous incipient wetness impregnation of the pre-evacuated carriers γ-Al_2O_3 and SiO_2 with an aqueous solution of metal precursors $Fe(NO_3)_3$ and $Cu(NO_3)_2$ of a required concentration followed by drying at 110 °C for 12 h in a drying oven. Then dry samples were subjected to thermal treatment in air at 300 °C for 4 h. The calcined samples were examined in the hydrogenation reaction without an additional reduction step. The calcination temperatures were selected in accordance with the data on thermogravimetry and differential thermal analysis (TG-DTA).[11,12] The monometallic catalysts with the same loading of metals were prepared by the incipient wetness impregnation of SiO_2 and Al_2O_3 for comparison of catalytic properties. Commercial γ-Al_2O_3 (S_{BET} = 270 m^2 g^{-1}; $V_{mesopore}$ = 0.46 cm^3 g^{-1}; $V_{micropore}$ = 0.005 cm^3 g^{-1}) and SiO_2 (KSKG trade mark, S_{BET} = 108 m^2 g^{-1}; D_{por} = 26 nm; V_{por} = 1.05 cm^3 g^{-1}) were used as carriers for bimetallic nanoparticles.

The investigation of the catalytic activity of the synthesized bimetallic Cu–Fe catalysts in the liquid-phase reaction of isoprenyl acetate (3-methyl-3-buten-1-yl acetate) hydrogenation was carried out in a 100 ml autoclave equipped with a probe-withdrawing valve at a temperature of 170 °C and H_2 pressure of 2 MPa in methanol medium for 6 h. A 4 mM isoprenyl acetate solution in methanol (15 ml) with decane as an internal standard and 0.10 g of a catalyst were added to the reactor. Before heating the autoclave was purged with hydrogen 3 times to exclude the presence of oxygen in the system. Samples of the reaction mixture were analyzed by gas-liquid chromatography with an internal standard method on a CrystaLux 4000M chromatograph using an Optima-1 (Macherey-Nagel) capillary column (30 m × 0.25 mm), a flame-ionization detector and mass spectrometry.

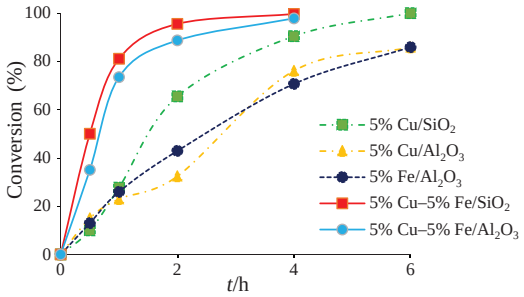

Figure 1 The dependence of the isoprenyl acetate conversion on the reaction time on the bimetallic Cu–Fe catalysts.

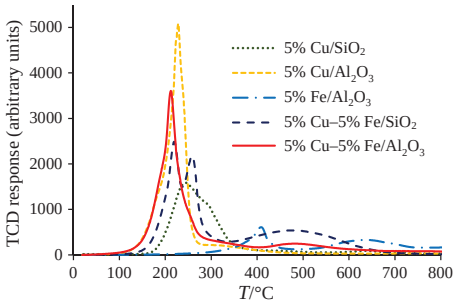

Figure 3 TPR–H_2 profiles of the mono- and bimetallic supported Cu–Fe catalysts.

with monometallic Cu and Fe samples (Figure 1). Also, the nature of the carrier affected the catalytic properties of the prepared bicomponent Cu–Fe systems. When using Al_2O_3 instead of SiO_2 as a support of the bimetallic 5% Cu–5% Fe catalyst, the selectivity has increased significantly. The best catalytic properties were found for the 5% Cu–5% Fe/Al_2O_3 bimetallic catalyst which provided a 98% isoprenyl acetate conversion in 4 h and the isoprenol selectivity of 82% (Figure 2).

A few methods can be applied to gain information about the electronic state of the supported metal in the bicomponent systems, catalyst phase composition and its microstructure. Studies of calcined mono- and bimetallic Cu–Fe samples were carried out by TPR–H_2 method to determine the interaction of two metals in bicomponent systems. The TPR–H_2 profiles revealed a different reduction behavior of the samples depending on the nature of the carrier (Figure 3). For the monometallic 5% Cu/Al_2O_3 sample there is one narrow symmetric peak at 229 °C which has been attributed to dispersed CuO phase reduction. The TPR curve of the bimetallic 5% Cu–5% Fe/Al_2O_3 catalyst is represented by a narrow intense peak with a small shoulder in the temperature range from 100 to 300 °C with a maximum at 215 °C, which is shifted to the low-temperature region relative to the monometallic copper-containing catalyst, and a wide peak at 400–600 °C. The deconvolution of the first peak and the calculated H_2/Fe and H_2/Cu molar ratios for this area (see Table 1) indicate the accelerating effect of Cu^0 on Fe^{3+} reduction and formation of a mixed oxide phases of copper and iron. The displacement of the TPR profile for the sample supported on Al_2O_3 to the lower temperature region is probably responsible for high dispersion of metal oxides. The second peak in the temperature range of 400–650 °C and a molar ratio of H_2/Fe equal to 0.89 refer to the reduction of Fe_3O_4 nanoparticles supported on aluminum oxide. In turn, the reduction of the monometallic 5% Fe/Al_2O_3 catalyst proceeds in two steps: Fe^{3+} is reduced to Fe^0 *via* Fe^{2+} in the range of 300–800 °C.[11–14] The TPR–H_2 profile of the SiO_2-supported Cu–Fe catalyst exhibited a different reducibility. The profile is represented by a double peak of lower intensity in the range 128–400 °C with a maximum at 221 °C in the region of reduction of silica-supported CuO and a maximum at 263 °C corresponding to a partial reduction of iron oxide phases. The peak in the temperature range of 400–700 °C with a maximum at 492 °C corresponds to the reduction of Fe^{2+} to Fe^0. Thus, in a bimetallic iron–copper catalyst there is a close contact interaction between the oxide phases of iron and copper, and Cu^0 phase contributes to easier reduction of Fe_2O_3. The accelerating effect of copper nanoparticles on the reducibility of Fe_2O_3 to Fe_3O_4 was described in works.[15–17]

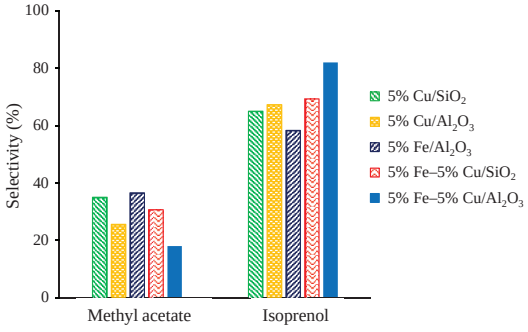

Figure 2 Selectivity of products at full conversion of isoprenyl acetate on mono- and bimetallic Cu–Fe catalysts.

According to the TPR–H_2 data, the hydrogenation reaction temperature of 180 °C contributes to the initial partial reduction of copper oxide during the reaction occurring on the calcined bimetallic 5% Cu–5% Fe/Al_2O_3 catalyst. The high selectivity of the Al_2O_3-supported bimetallic catalyst is probably due to the high dispersion of Fe_2O_3, CuO, and Cu^0 nanoparticles with strong contact interactions between the metals.

The electronic state of the metals in the prepared catalysts was studied using the DRIFTS-CO spectroscopy. The DRIFTS-CO spectra (Figure 4) recorded for the bimetallic 5% Cu–5% Fe/SiO_2 catalyst showed a low-intensity band at 2360 cm^{-1} corresponding to a Fe^{2+}–CO_2 complex formed as a result of Fe^{3+} reduction by CO[4,16] and an intense line at 2127 cm^{-1} that can be assigned to the stretching vibrations of CO molecules adsorbed on Cu^+ cations.[18,19] Cu^+ cations can be formed *via* Cu^{2+} cations reduction by CO.[20,21] According to the DRIFTS-CO data for the Al_2O_3-supported Cu–Fe sample (Figure 4), deposition of copper oxide nanoparticles on Al_2O_3 resulted in a shift of the band of Cu^+–CO to 2118 cm^{-1}, which could be explained by the formation of electron-deficient copper species ($Cu^{\delta+}$–CO).[21,22] The presence of this band likely indicates a strong interaction of copper and iron species in the 5% Cu–5% Fe/Al_2O_3 catalyst, that is also consistent with the TPR–H_2 results for this catalyst. The band position at 2190 cm^{-1} agrees with the assignment to CO adsorbed on Al^{3+} cations.[23]

TEM data confirm the assumption about the presence of highly dispersed oxide phase in the bimetallic sample deposited on aluminum oxide (Figure 5). TEM micrographs of the 5% Cu–5% Fe/Al_2O_3 catalyst show a needle-like structure of the

Table 1 Hydrogen consumption data for the mono- and bimetallic Fe–Cu catalysts.

Catalyst	T/°C	T_{max}/°C	H_2/Cu mol/mol	H_2/Fe mol/mol	H_2 uptake/ mmol g^{-1}
5% Cu/SiO_2	150–400	236	1.13	–	0.89
5% Cu/Al_2O_3	100–400	229	1.97	–	1.52
5% Fe/Al_2O_3	300–800	416 628	–	0.83	0.23 0.51
5% Cu– 5% Fe/SiO_2	128–700	223 260 470	0.69	1.34	0.54 0.49 0.71
5% Cu– 5% Fe/Al_2O_3	100–600	215 486	1.01	0.88	1.24 0.33

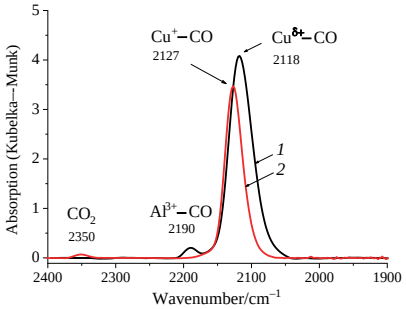

Figure 4 DRIFTS-CO study of the bimetallic Cu–Fe catalysts: (*1*) 5% Cu–5% Fe/Al_2O_3, (*2*) 5% Cu–5% Fe/SiO_2.

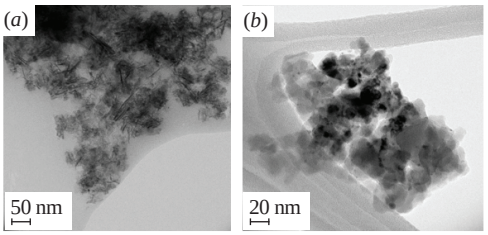

Figure 5 TEM images of the prepared bimetallic samples: (*a*) 5% Cu–5% Fe/Al_2O_3; (*b*) 5% Cu–5% Fe/SiO_2.

alumina carrier as well as supported particles with the prevailing average size of 3.5 nm and aggregates of particles with a size of 10–13 nm. However, large NPs with a size of about 8.5 nm and particle aggregates above 20 nm can be seen in the TEM image of the SiO_2-supported Cu–Fe catalyst. Apparently the metal interaction with alumina is stronger than with silica.

Thus, the best catalytic properties in the selective hydrogenation of unsaturated ether were obtained in the presence of the synthesized bimetallic 5% Cu–5% Fe/Al_2O_3 catalyst, which allowed us to achieve 98% conversion and 82% isoprenol selectivity for 4 h. The high selectivity of the bimetallic Cu–Fe catalyst based on Al_2O_3 is probably due to the high dispersion of Fe_2O_3, CuO and Cu^0 nanoparticles with strong contact interactions between metals.

This work was supported by the Council on grants of the President of the Russian Federation MK-3311.2021.1.3 in part related to hydrogenation of ester and catalysts synthesis and by the Ministry of Science and Higher Education of the Russian Federation (grant no. 075-15-2021-591) in the part related to catalyst characterization.

References

1 R. K. Srivastava, N. P. Shetti, K. R. Reddy and T. M. Aminabhavi, *Environ. Chem. Lett.*, 2020, **18**, 1049.
2 N. S. Hassan, A. A. Jalil, C. N. C. Hitam, D. V. N. Vo and W. Nabgan, *Environ. Chem. Lett.*, 2020, **18**, 1625.
3 W. Runguphan and J. D. Keasling, *Metab. Eng.*, 2014, **21**, 103.
4 I. V. Deily, I. L. Simakova, N. Ravasio and R. Psaro, *Appl. Catal., A*, 2009, **357**, 170.
5 J. V. Gerpen, *Fuel Process Technol.*, 2005, **86**, 1097.
6 J. Kim, E. E. K. Baidoo, B. Amer, A. Mukhopadhyay, P. D. Adams, B. A. Simmons and T. S. Lee, *Metab. Eng.*, 2021, **64**, 154.
7 S. Pandey, S. C. Phulara, A. Jha, P. S. Chauhan, P. Gupta and V. Shukla, *Int. J. Food Sci. Nutr.*, 2019, **70**, 595.
8 A. S. Belousov, A. L. Esipovich, E. A. Kanakov and K. V. Otopkova, *Sustainable Energy Fuels*, 2021, **5**, 4512.
9 M. Sánchez, G. Torres and V. Mazzieri, *J. Chem. Technol. Biotechnol.*, 2017, **92**, 27.
10 A. A. Strekalova, A. A. Shesterkina and L. M. Kustov, *Catal. Sci. Technol.*, 2021, **11**, 7229.
11 O. Kirichenko, G. Kapustin, V. Nissenbaum, A. Strelkova, E. Shuvalova, A. Shesterkina and L. Kustov, *J. Therm. Anal. Calorim.*, 2018, **134**, 233.
12 L. M. Kustov, A. L. Tarasov, V. D. Nissenbaum and A. L. Kustov, *Mendeleev Commun.*, 2021, **31**, 376.
13 O. Kirichenko, G. Kapustin, V. Nissenbaum, I. Mishin and L. Kustov, *J. Therm. Anal. Calorim.*, 2014, **118**, 749.
14 N. Lingaiah, N. S. Babu, R. Gopinath, P. S. S. Reddy and P. S. S. Prasad, *Catal. Surv. Asia*, 2006, **10**, 29.
15 L. He, X. Gong, L. Ye, X. Duan and Y. Yuan, *J. Energy Chem.*, 2016, **25**, 1038.
16 D. Santos Monteiro and M. O. Guarda Souza, *J. Therm. Anal. Calorim.*, 2016, **123**, 955.
17 E. A. Redina, G. I. Kapustin, O. P. Tkachenko, A. A. Greish and L. M. Kustov, *Catal. Sci. Technol.*, 2021, **11**, 5881.
18 R. Lu, D. Mao, J. Yu and Q. Guo, *J. Ind. Eng. Chem.*, 2015, **25**, 338.
19 R. Xu, Z. Ma, C. Yang, W. Wei, W. Li and Y. Sun, *J. Mol. Catal. A: Chem.*, 2004, **218**, 133.
20 Tz. Venkov and K. Hadjiivanov, *Catal. Commun.*, 2003, **4**, 209.
21 J. Schumann, J. Kröhnert, E. Frei, R. Schlögl and A. Trunschke, *Top. Catal.*, 2017, **60**, 1735.
22 C. Sun, D. Mao, L. Han and J. Yu, *Catal. Commun.*, 2016, **84**, 175.
23 M. A. Larrubia Vargas, G. Busca, U. Costantino, F. Marmottini, T. Montanari, P. Patrono and G. Ramis, *J. Mol. Catal. A: Chem.*, 2007, **266**, 188.

Received: 18th March 2022; Com. 22/6830